Static and Dynamic Light Scattering of a Nematic Side-Group Polysiloxane

Jürgen Schmidtke, Werner Stille,* and Gert Strobl

Fakultät für Physik, Albert-Ludwigs-Universität Freiburg, Hermann-Herder-Strasse 3, D-79104 Freiburg, Germany

Received July 21, 1999; Revised Manuscript Received February 9, 2000

ABSTRACT: Static and dynamic light-scattering experiments on a nematic side-group polymer are described. Using two different scattering geometries, the depolarized scattering due to thermally excited fluctuations of the nematic director was analyzed. The relaxation rates and strengths show the q dependence known from low molar mass nematics. Values for the bend and splay elastic constants and the associated effective viscosities have been obtained for a wide temperature range. The elastic constants are of the same order of magnitude as those of low molar mass nematics, whereas the presence of the polymer backbone results in drastically increased effective viscosities. In the isotropic phase near-critical order parameter fluctuations are observed; scattering intensities and relaxation rates are found to be in accordance with the Landau−de Gennes description.

Introduction

Dynamic light-scattering analysis of thermally excited director fluctuations is a powerful tool to investigate the viscoelastic properties of nematic liquid crystals. Several studies on low molar mass compounds (see, e.g., refs 1 and 2) and nematic polymers of various architectures dissolved in nematic solvents[3−5] have been reported. We now performed static and dynamic light-scattering experiments on a nematic side-group polysiloxane.

The distortions of the director field result in two scattering components, being a combination of bend−splay and bend−twist distortions, respectively. The differential cross section per unit volume, i.e., the Rayleigh ratio, is given by[6]

$$R = \frac{1}{V}\frac{\mathrm{d}\sigma}{\mathrm{d}\Omega} = \left(\frac{\pi\Delta\epsilon}{\lambda^2}\right)^2 k_\mathrm{B}T \sum_{\nu=1,2} \frac{p_\nu(\mathbf{q})}{K_{\nu\nu}{q_\perp}^2 + K_{33}{q_{||}}^2} \quad (1)$$

where $K_{\nu\nu}$, $\nu = 1$, 2, and 3, denote the Frank elastic constants of the splay, twist, and bend modes, $\Delta\epsilon$ the anisotropy of the dielectric constant, λ the wavelength of the light in vacuo and $q_{||}$, $q_\perp$ the components of the scattering vector $\mathbf{q}$ parallel and perpendicular to the director. $p_\nu(\mathbf{q})$ is a geometric factor, depending on the scattering geometry: Most conveniently, it is formulated in the frame of a Cartesian coordinate system $\{\mathbf{e}_1,\mathbf{e}_2,\mathbf{e}_0\}$, with the unit vector $\mathbf{e}_0$ denoting the optical axis, and $\mathbf{e}_2 = (\mathbf{e}_0 \times \mathbf{q})/|\mathbf{e}_0 \times \mathbf{q}|$, $\mathbf{e}_1 = (\mathbf{e}_2 \times \mathbf{e}_0)/|\mathbf{e}_2 \times \mathbf{e}_0|$. The factor $p_\nu(\mathbf{q})$ then reads

$$p_\nu = (i_\nu f_0 + i_0 f_\nu)^2 \quad (2)$$

with i_ν and f_ν, $\nu = 1$, 2, and 0, denoting the components of the polarization of the incident and scattered light.

Photon correlation analysis yields the relaxation rates ${\tau_\nu}^{-1}$ of the two deformation modes

$${\tau_\nu}^{-1}(\mathbf{q}) = \frac{K_{33}{q_{||}}^2 + K_{\nu\nu}{q_\perp}^2}{\eta_\nu(\mathbf{q})} \quad (3)$$

with effective viscosities

$$\eta_1(\mathbf{q}) = \gamma_1 - \frac{({q_\perp}^2\alpha_3 - {q_{||}}^2\alpha_2)^2}{{q_\perp}^4\eta_\mathrm{b} + {q_\perp}^2{q_{||}}^2(\alpha_1 + \alpha_3 + \alpha_4 + \alpha_5) + {q_{||}}^4\eta_\mathrm{c}} \quad (4)$$

$$\eta_2(\mathbf{q}) = \gamma_1 - \frac{{\alpha_2}^2{q_{||}}^2}{{q_\perp}^2\eta_\mathrm{a} + {q_{||}}^2\eta_\mathrm{c}} \quad (5)$$

where the α_i values denote the Leslie viscosity coefficients, γ_1 denotes the rotational viscosity and η_a, η_b, and η_c denote the Miesowicz viscosities. In our experiment, the sample was centered as a homogeneously orientated film in the light-scattering setup. We analyzed the depolarized scattering using two different scattering geometries.

1. Alignment of the director in the scattering plane and approximately parallel to the scattering vector (Figure 1a): In this case ($q_{||} \gg q_\perp$ and $p_1(\mathbf{q}) = 0$), mode 1 in eq 1 vanishes, and mode 2 reduces to pure bend

$$\frac{1}{V}\frac{\mathrm{d}\sigma}{\mathrm{d}\Omega} = \left(\frac{\pi\Delta\epsilon}{\lambda^2}\right)^2 k_\mathrm{B}T\,\frac{{f_0}^2(\mathbf{q})}{K_{33}q^2} \quad (6)$$

The bend mode relaxation rate ${\tau_\mathrm{bend}}^{-1}$ is determined by the ratio of the elastic constant K_{33} and the effective bend viscosity η_bend:

$${\tau_\mathrm{bend}}^{-1} = \frac{K_{33}}{\eta_\mathrm{bend}}q^2 \quad (7)$$

$$\eta_\mathrm{bend} = \gamma_1 - \frac{{\alpha_2}^2}{\eta_c} \quad (8)$$

2. Alignment of the director perpendicular to the scattering plane (Figure 1b): In this case ($q_{||} = 0$) the bend contributions in eqs 1−5 vanish and a superposition of splay and twist mode fluctuations is detected, weighed by the angular dependent factors $p_\nu = {f_\nu}^2$. In the investigated q range, the splay contribution is predominant. The differential cross section then ap-

10.1021/ma9911997 CCC: $19.00
Published on Web 03/29/2000

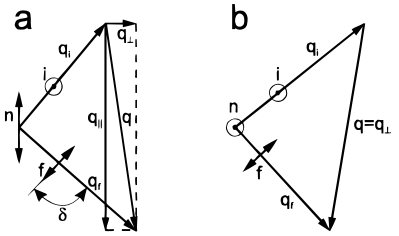

Figure 1. Sketch of the scattering geometries for bend mode detection (a) and splay mode detection (b): n director; q_i, q_f wavevectors of incident and scattered rays; i, f polarizations of incident and scattered rays; **q** scattering vector with components $q_{||}$, $q_\perp$ parallel and perpendicular to the director. In the bend mode geometry, due to the optical anisotropy the scattered ray's wavevector and electric field are not perpendicular ($\delta \neq \pi/2$).

proximately reduces to

$$\frac{1}{V}\frac{\mathrm{d}\sigma}{\mathrm{d}\Omega} = \left(\frac{\pi\Delta\epsilon}{\lambda^2}\right)^2 k_B T \frac{{f_1}^2}{K_{11}q^2} \tag{9}$$

The splay mode relaxation rate ${\tau_{\mathrm{splay}}}^{-1}$ is determined by the ratio of the elastic constant K_{11} and the effective splay viscosity η_{splay}

$${\tau_{\mathrm{splay}}}^{-1} = \frac{K_{11}}{\eta_{\mathrm{splay}}}q^2 \tag{10}$$

$$\eta_{\mathrm{splay}} = \gamma_1 - \frac{{\alpha_3}^2}{\eta_b} \tag{11}$$

The second terms in eqs 8 and 11 originate from a backflow effect, a reduction of the effective value of the rotational viscosity, because the reorientation of the director is supported by the convective flow associated with the deformation modes.

Experimental Section

The polymer under investigation has the structural unit

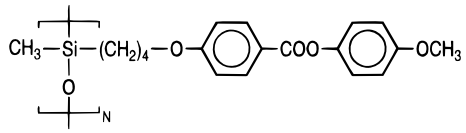

It has a broad molecular weight distribution with an average degree of polymerization $P_w \approx 100$. The glass transition and nematic−isotropic transition temperatures are $T_g \approx 15$ °C and $T_{NI} \approx 99$ °C, respectively. The samples were prepared as homogeneously oriented films between two polyimide-coated and subsequently rubbed glass slides separated by Kapton spacers (thickness 25 μm). Uniform director orientation was supported by annealing the sample in a magnetic field of about 1.2 T at 75 °C for about 20 h. Figure 2 shows a sketch of the light-scattering setup. The sample cell was centered in a refractive index matching bath (silicone oil WACKER AK50). Temperature was controlled with accuracy better than 0.1 K. A commercial goniometer (ALV−Langen) with an argon-ion laser operating at a wavelength of 488 nm was used. For selection of the VH scattering component, the experiment was equipped with appropriately adjusted polarizers in front of the scattering cell and in front of the detector. The photon correlation analysis was performed using an ALV-5000/E Multiple Tau Digital Correlator.

In photon correlation spectroscopy, the normalized intensity autocorrelation function

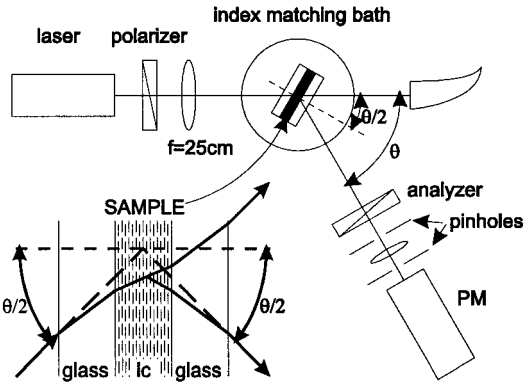

Figure 2. Schematic representation of the light-scattering setup.

$$G_2(t) = \langle n(0)n(t)\rangle/\langle n(0)\rangle^2 - 1 \tag{12}$$

is computed from the detected photon counts $n(t)$ at time increments t, the brackets denoting a time average. In our experiments, a coherently scattered static contribution due to sample heterogeneities was added to the fluctuating scattering intensity. Because of the interference of the two scattering components, the experimental intensity correlation function is related to the electric field correlation function $g_1(t)$ by a generalized Siegert relation[7]

$$G_2(t) = f\,(\alpha^2 g_1(t)^2 + 2\alpha(1-\alpha)g_1(t)) \tag{13}$$

where the factor α denotes the ratio $\langle I_f\rangle/\langle I_{tot}\rangle$ of the mean fluctuating intensity contribution and the mean total intensity. The field coherence factor $f < 1$ accounts for the averaging effect due to the finite scattering volume and detector aperture. The static structure factor of the nematic fluctuations is derived from the fluctuating contribution $\langle I_f\rangle = \alpha\langle I_{tot}\rangle$ to the detected total scattering intensity. The experimental correlation functions were fitted according to eq 13, using for the field correlation function the empirical Williams−Watts function $g_1(t) = \exp(-(t/\tau_{ww})^{\beta})$. Values of the exponent $\beta < 1$ are indicating a finite width of the relaxation time distribution. The mean relaxation time and the width of the relaxation time distribution was computed using the relations[8] $\langle\tau\rangle = \tau_{ww}\Gamma(1/\beta)/\beta$ and $\Delta\tau/\langle\tau\rangle = (\beta\Gamma(2/\beta)/\Gamma^2(1/\beta) - 1)^{1/2}$, Γ denoting the gamma function.

At a given scattering angle θ, pure bend mode detection was approximately achieved by rotating the sample cell by an angle $\theta/2$ in the same direction as the goniometer. The small mismatch in $\boldsymbol{q}||\boldsymbol{n}$ alignment due to the different indices of refraction for the vertically polarized incoming beam and the horizontally polarized scattered beam leads to a small twist mode contribution. $(q_\perp/q_{||})^2$ is largest for small scattering vectors and drops drastically with increasing scattering angle θ. In our experiments, it never exceeded 0.049. At perpendicular orientation of the director with respect to the scattering plane, a combination of splay and twist fluctuations is detected, depending on the ratio of the polarization factors $p_{1,2}$. The splay contribution is predominant at intermediate q values. Pure splay detection was approximately achieved by restriction on a q range satisfying $p_2/p_1 < 0.1$.

In both scattering geometries described in the Introduction, sample rotation by an angle $\theta/2$ proved to be favorable for absolute intensity measurements: Due to the high symmetry of the paths of incoming and scattered rays, θ-dependent readjustments of the sample position were not necessary. Besides, the θ-independent cross section of the scattering volume as seen by the detector guarantees a constant value of the field coherence factor f, thus simplifying data evaluation according to eq 13.

For intensity calibration, count rates of the critical scattering of a low molecular weight LC in the isotropic phase were recorded for samples prepared as a thin film and in a

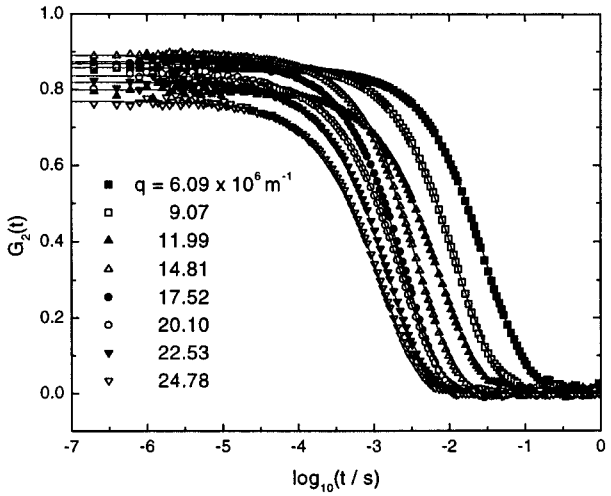

Figure 3. Experimental correlation functions $G_2(t)$, obtained in the bend mode geometry at 82.9 °C. The solid lines are fitted curves.

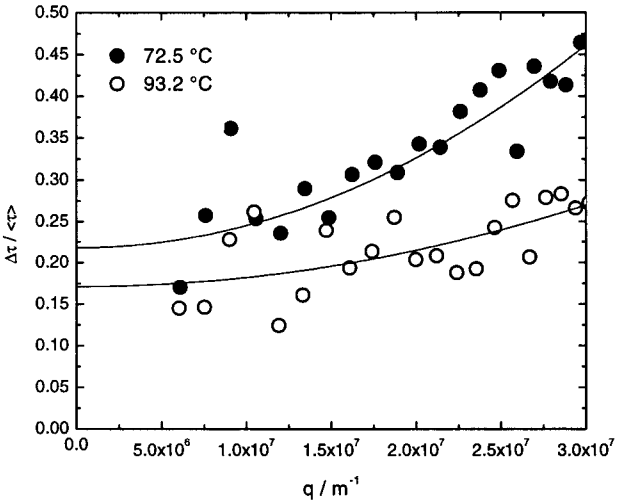

Figure 4. q dependence of the width of the relaxation rate distribution $\Delta\tau/\langle\tau\rangle$, obtained for the bend mode.

conventional light-scattering cuvette and compared with the scattering intensity of toluene, whose Rayleigh ratio is known from the literature.[9] The obtained intensities were corrected for the angular dependent transmittances of the oil/glass and glass/sample interfaces for the incoming and scattered beam, respectively. Also taken into account was the scattered beam's solid angle distortion on traversing the glass interfaces.[10] In determination of these quantities as well as of the polarization factors p_ν the sample's optical anisotropy was fully taken into account.

Results

In Figure 3, we present typical correlation functions obtained in the bend mode geometry at several scattering vectors. In contrast to low molecular weight LCs, no pure exponential relaxation is observed. The width $\Delta\tau/\langle\tau\rangle$ of the relaxation time distribution as derived from the Williams−Watts exponent β shows the q dependence depicted in Figure 4. The observed variation may indicate that, on increasing the length scale, the fluctuations average more and more efficiently over microscopic heterogeneities. At increasing temperature, the disturbing influence of the heterogeneities diminishes. The finite width of the relaxation rate distribution in the limit $q = 0$ may be attributed to imperfect overall parallel alignment of the director.

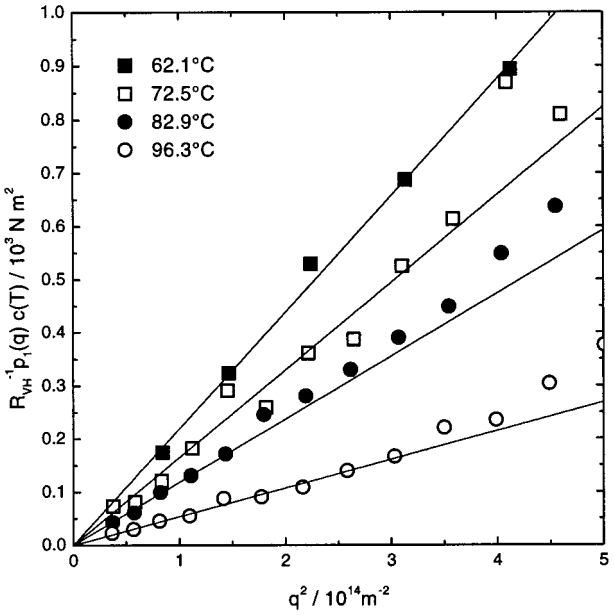

Figure 5. q^2 dependence of the inverse Rayleigh ratio (p_1, polarization factor; $c(T) = (\pi\Delta\epsilon/\lambda^2)^2 k_B T$)). Results obtained in bend mode geometry.

The inverse Rayleigh ratio, corrected for the geometric factor p_ν, shows a linear q^2 dependence, the slope being related to the selected mode's elastic constant. Examples obtained in bend mode geometry are shown in Figure 5. For large scattering vectors, small deviations from the linear q^2 dependence to higher values can be observed, which suggests some stiffening effect on approaching small length scales. Evaluation of the scattering intensities yielded the temperature dependence of the bend and splay elastic constants depicted in Figure 6a. The obtained values are of the same order of magnitude as those of typical low molar mass nematics, in accordance with results from Freedericksz experiments on other nematic side chain polymers.[11] Remarkably, the two elastic constants almost coincide for all temperatures.

The obtained mean relaxation rates show the linear q^2 dependence as predicted by eqs 7 and 10. Results obtained in the bend mode geometry are depicted in Figure 7. Again, at large scattering vectors small deviations show up, consistent with the stiffening of the elastic restoring forces on small length scales as suggested by the q^2 dependence of the inverse Rayleigh ratio.

The slope in the plot of the relaxation rate vs q^2 yields the ratio of the selected mode's elastic constant and effective viscosity. The values obtained for the two selected modes are shown in Figure 6b. Obviously the temperature dependence is governed by the viscosity. Near the transition to the isotropic phase the relaxation rates of the bend and splay modes pass over maxima, which are located in the two phase region. Division of the slope of $\tau^{-1}(q^2)$ by the respective elastic constant yields the effective viscosity associated with the selected mode. The values thus obtained for η_{bend} and η_{splay} are depicted in Figure 6c. They show a substantial decrease within the investigated temperature range. Furthermore, they are several orders of magnitude higher than typical values obtained for low molar mass nematics.

In the two-phase region above 95 °C a superposition of director fluctuations in the nematic phase and critical order parameter fluctuations in the isotropic phase is

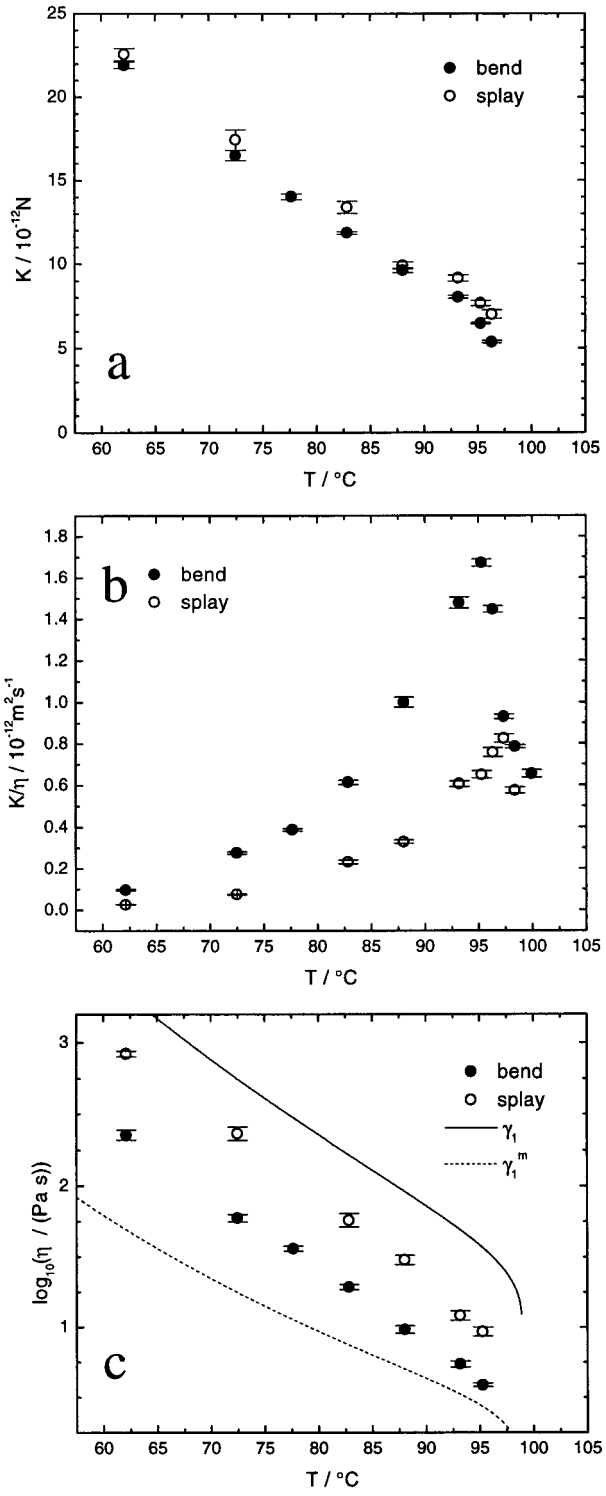

Figure 6. Temperature dependencies of the splay and bend elastic constants (a), the elastic constant-viscosity ratio (b), and the associated effective viscosities (c). Rotational viscosity γ_1 and contribution of the nematic matrix γ_1^m (in part c).

detected. Figure 8 presents correlograms measured in this region, and they show a two-step decay. The scattering intensities and decay rates of the order parameter fluctuations did not show a significant q dependence, suggesting short correlation lengths of the fluctuations comparable to those in low molecular weight compounds (typically ≈10 nm). As shown in Figure 9, approaching the nematic−isotropic transition region a critical slowing down is observed. It is associated with an increase of the scattering intensity. Figure 10 depicts the temperature dependence of the inverse scattering intensity. The values in the two phase region (first two data points) were obtained at large scattering vectors, where the correlation functions showed no significant contribution due to director fluctuations.

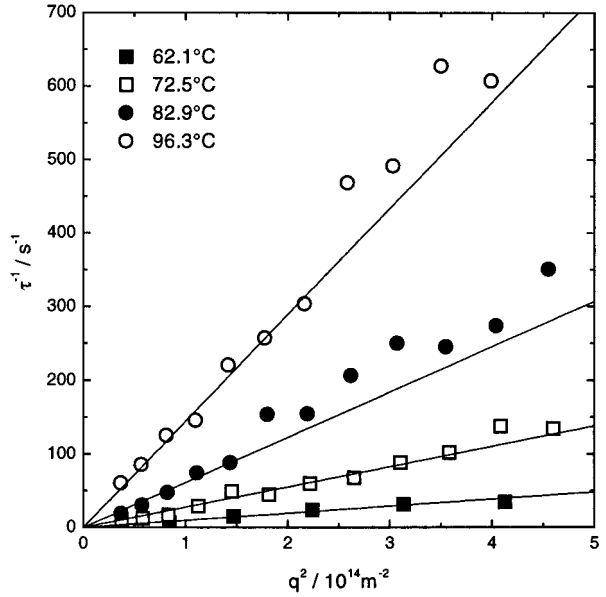

Figure 7. q^2 dependence of the mean decay rates, obtained in bend mode geometry at different temperatures.

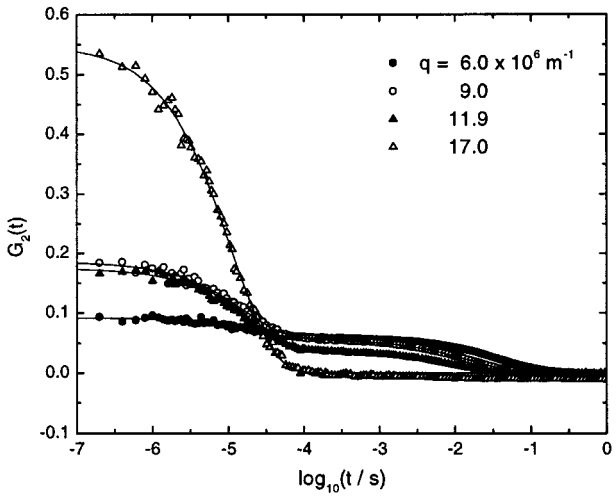

Figure 8. Correlation functions $G_2(t)$ obtained in the two-phase region ($T = 100.0$ °C) showing a superposition of nematic director fluctuations and critical order parameter fluctuations. The solid lines are fitted according to eq 13, using for the field correlation function a weighed sum of two Williams−Watts functions.

Discussion

There are two reasons for the drastic increase of the viscosities in the nematic phase compared to those of low molar mass nematogens. First, the presence of the polymer yields an upward shift of the glass transition temperature. Second, if the chain conformation is anisotropic, reorientation of the director requires rearrangement of the backbone chains together with translational motion of the mesogens. The influence of both effects on the rotational viscosity γ_1 has been demonstrated and analyzed in previous studies, where we combined dielectric relaxation spectroscopy, giving the rotational

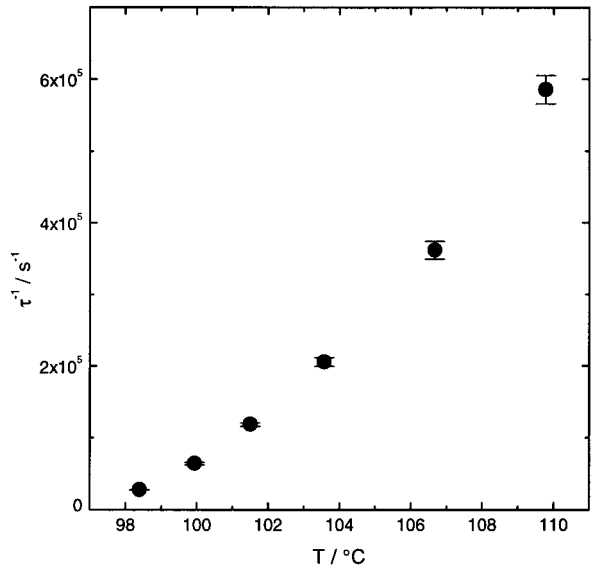

Figure 9. Temperature dependence of the relaxation rate of the order parameter fluctuations in the isotropic phase.

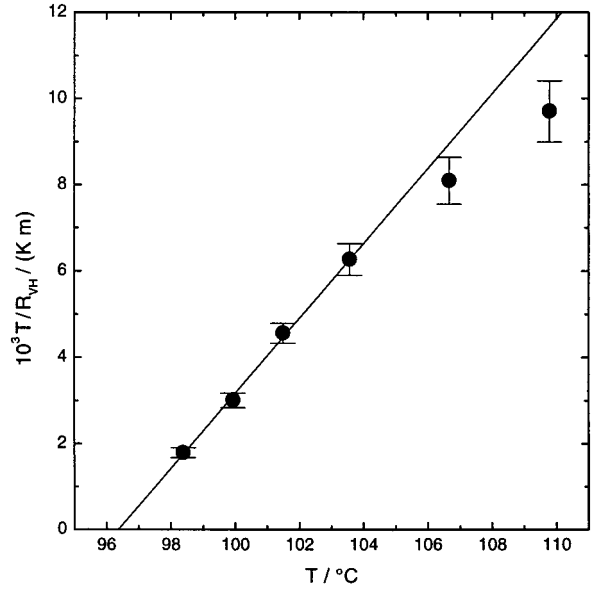

Figure 10. Temperature dependence of the ratio T/R_{VH}.

diffusion coefficient D_r, and director reorientation experiments determining γ_1.[12,13] Experiments were carried out for the same LC-polymer as studied in the present paper and yielded the temperature dependencies of the rotational diffusion constant D_r and of the ratio $\gamma_1/\Delta\chi$, which includes the anisotropy of the diamagnetic susceptibility $\Delta\chi$. If we now choose, for an estimate, $\Delta\chi$ values obtained in our group for a low molecular weight compound with similar chemical structure ("C_6C_3" in ref 14), we may roughly calculate the rotational viscosity γ_1. The temperature dependence thus obtained is shown in Figure 6c as a continuous line. It is located above η_{splay} and η_{bend}, which may be understood, regarding eqs 8 and 11, as being due to the backflow effect.

According to a theoretical treatment of Brochard,[15] in a nematic system containing polymers the rotational viscosity is the sum of a contribution γ_1^m of the nematic matrix and a contribution $\Delta\gamma_1$ due to the presence of the chains. An explicit expression for γ_1^m may be taken from a work of Raviol et al.,[16] carried out on low molar mass nematogens. It relates the rotational viscosity to the rotational diffusion constant by

$$\gamma_1 = \frac{\rho k_B T}{D_r(S)} g(S) \tag{14}$$

Experimental results for various low molecular weight compounds were well described by using for the function $g(S)$ the expression derived by Marrucci[17]

$$g(S) = 3S^2/(2+S) \tag{15}$$

and taking into account the tube dilation effect, as discussed by Doi for solutions of rigid rods,[18] writing

$$D_r(S) = D_r(0)/(1\text{-}S^2)^2 \tag{16}$$

where $D_r(0)$ denotes the rotational diffusion constant in an isotropic environment. If we apply eq 14 to deduce from the previously measured values of D_r the temperature dependence of γ_1^m, we obtain the dashed line also included in Figure 5c. It is located below η_{splay} and η_{bend}.

For a further discussion of the results, again one can refer to the theory of Brochard,[15] describing the changes of viscous properties induced by the presence of the chains. The anisotropic interaction between backbone chain and nematic matrix in general results in an anisotropic chain conformation, which may be prolate or oblate, depending on the mesogenic species, spacer length, and degree of polymerization. This has been shown in a series of small-angle neutron[19−22] and X-ray scattering[23] experiments. Brochard derived expressions for the additional contributions to the rotational and Miesowicz viscosities due to the translational motion of the polymer. The theory, originally derived for dilute solutions of polymer chains in a nematic solvent, has been successfully used for the description of viscosity coefficients of dilute solutions of LC-polymers in nematic solvents[4,24] and also of nematic polymer melts.[13] The expressions derived for the viscosity increments read

$$\Delta\eta_b = \frac{ck_BT}{N} \frac{R_\perp{}^4}{D_\perp R_{||}{}^2 + D_{||} R_\perp{}^2} \tag{17}$$

$$\Delta\eta_c = \frac{ck_BT}{N} \frac{R_{||}{}^4}{D_\perp R_{||}{}^2 + D_{||} R_\perp{}^2} \tag{18}$$

$$\Delta\gamma_1 = \frac{ck_BT}{N} \frac{(R_\perp{}^2 - R_{||}{}^2)^2}{D_\perp R_{||}{}^2 + D_{||} R_\perp{}^2} \tag{19}$$

$$\Delta\gamma_2 = \frac{ck_BT}{N} \frac{R_\perp{}^4 - R_{||}{}^4}{D_\perp R_{||}{}^2 + D_{||} R_\perp{}^2} \tag{20}$$

where c is the monomer concentration, N is the degree of polymerization, $R_{||}$ and $R_\perp$ are the radii of gyration parallel and perpendicular to the director (with $R_{||}{}^2 + 2R_\perp{}^2 = R^2$), and $D_{||}$ and $D_\perp$ are the monomer diffusion constants for movement parallel and perpendicular to the director, respectively. The Leslie coefficients α_2 and α_3 included in the expressions for the effective viscosities measured in our experiment can be expressed in terms of the rotational viscosities γ_1 and γ_2 using the relations $\alpha_2 = {}^1/_2(\gamma_2 - \gamma_1)$ and $\alpha_3 = {}^1/_2(\gamma_2 + \gamma_1)$. The effective viscosities then read (the superscript m denotes the

mesogenic contributions, and $b = (D_\perp R_{||}^2 + D_{||} R_\perp^2)^{-1} ck_BT/N$)

$$\eta_{bend} = \gamma_1^m + b(R_\perp{}^2 - R_{||}{}^2)^2 - \frac{(\alpha_2^m + b(R_\perp{}^2 R_{||}{}^2 - R_{||}{}^4))^2}{\eta_c^m + bR_{||}{}^4} \quad (21)$$

and

$$\eta_{splay} = \gamma_1^m + b(R_\perp{}^2 - R_{||}{}^2)^2 - \frac{(\alpha_3^m + b(R_\perp{}^4 - R_\perp{}^2 R_{||}{}^2))^2}{\eta_b^m + bR_\perp{}^4} \quad (22)$$

It is interesting to study the limiting cases of spherical, extremely prolate and extremely oblate coil conformations, respectively. For spherical coils ($R_{||} = R_\perp$), the chain contributions to γ_1 and γ_2 vanish, and the effective viscosities reduce to

$$\eta_{bend} = \gamma_1^m - (\alpha_2^m)^2/(\eta_c^m + b\,R^4/9) \quad (23)$$

$$\eta_{splay} = \gamma_1^m - (\alpha_3^m)^2/(\eta_b^m + b\,R^4/9) \quad (24)$$

Thus, we obtain $\eta_{bend} \le \gamma_1^m$ and $\eta_{splay} \le \gamma_1^m$, which is in contradiction to our results. Hence, we have a clear indication for the anisotropy of the chains. In the case of a rodlike chain ($R_{||} \gg R_\perp$), one finds

$$\eta_{bend} \approx \gamma_1^m + \eta_c^m + 2\alpha_2^m = \eta_b^m \quad (25)$$

$$\eta_{splay} \approx \gamma_1^m + bR_{||}^4 = \gamma_1 \quad (26)$$

In the case of a disklike chain ($R_{||} \ll R_\perp$), one finds

$$\eta_{bend} \approx \gamma_1^m + bR_\perp{}^4 = \gamma_1 \quad (27)$$

$$\eta_{splay} \approx \gamma_1^m + \eta_b^m - 2\alpha_3^m = \eta_c^m \quad (28)$$

Thus, in both cases of extreme chain anisotropy, one of the two effective viscosities retains a low value, determined by viscosity coefficients of the nematic matrix, while the other one behaves asymptotically like the rotational viscosity γ_1. The experimental result $\eta_{bend} < \eta_{splay} < \gamma_1$ indicates a prolate chain conformation. Though, the enhanced values of the bend viscosity coefficient with respect to the coefficient γ_1^m (with $\eta_{bend}/\gamma_1^m > 4$ at low temperatures) cannot quantitatively explained in the framework of the Brochard approach.

The order parameter fluctuations in the isotropic phase can be discussed using the phenomenological Landau−de Gennes description.[6] It gives for the scattering intensity a temperature dependence

$$R_{VH} \sim \frac{k_BT}{a\,(T - T_c^*)} \quad (29)$$

For low molecular weight nematics, the critical temperature T_c^* is typically located about 1 K below the transition temperature T_{NI}. Indeed, near the transition we find a linear temperature dependence of T/R_{VH}.

For the relaxation rate Γ the theory predicts

$$\Gamma = a(T - T_c^*)/\nu \quad (30)$$

where ν denotes the viscosity for relaxation of the orientational order. Combining eqs 29 and 30, the temperature dependence of the viscosity ν can be extracted: $\nu \sim T\tau/R_{VH}$. The result depicted in Figure 11 indicates an Arrhenius-type behavior $\nu \sim \exp(-E/(k_BT))$. The obtained value $E/k_B \approx 1.8 \times 10^4$ K is quite high compared to typical results for low molecular weight nematics (e.g., $E/k_B = 3.68 \times 10^3$ K for MBBA[25]). One should keep in mind, however, that, strictly speaking, the viscosity obeys a Vogel−Fulcher law, and a high value for the apparent activation energy E may just be due to the higher glass transition temperature of the polymer ($T_g = 15$ °C).

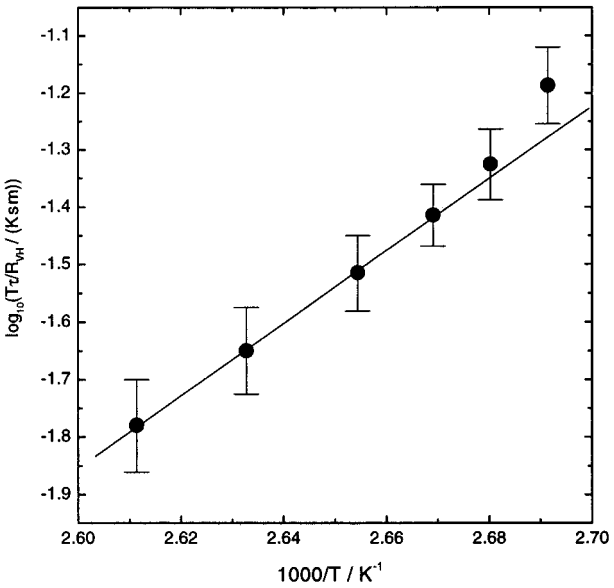

Figure 11. Arrhenius plot of $T\tau/R_{VH}$, giving the temperature dependence of the viscosity ν associated with the orientational relaxation in the isotropic phase.

Conclusions

From the foregoing discussion we see that in many respects the investigated polymer's viscoelastic properties probed by static and dynamic light scattering are quite similar to those of low molecular weight nematics, i.e., the q dependencies of relaxation rates and strengths and the numerical values for the selected modes' elastic constants. Slight deviations at large scattering vectors may indicate enhanced elastic restoring forces on small length scales. Strongly affected by the presence of the polymer backbone are the effective viscosities, which are several orders of magnitude higher than typical values for low molecular weight materials. The scattering due to near-critical pretransitional order parameter fluctuations in the isotropic phase shows a behavior similar to that observed for low molecular weight compounds. The results are in accordance with the phenomenological Landau−de Gennes description.

Acknowledgment. Support of this work by the Deutsche Forschungsgemeinschaft (Sonderforschungsbereich 428, Freiburg) is gratefully acknowledged.

References and Notes

(1) Orsay Liquid Crystal Group *Phys. Rev. Lett.* **1969**, *22*, 1361−1363.
(2) Hirakata, J.; Chen, G.; Toyooka, T.; Kawamoto, S.; Takezoe, H.; Fukuda, A. *Jpn. J. Appl. Phys.* **1986**, *25*, 607−610.
(3) Gu, D.; Jamieson, A. M.; Rosenblatt, Ch.; Tomazos, D.; Lee, M.; Percec, V. *Macromolecules* **1991**, *24*, 2385−2390.

(4) Gu, D.; Jamieson, A. M.; Kawasumi, M.; Lee, M.; Percec, V. *Macromolecules* **1992**, *25*, 2151−2155.
(5) Chen, F.-L.; Jamieson, A. M.; Kawasumi, M.; Percec, V. *J. Polym. Sci., Polym. Phys. Ed.* **1995**, *33*, 1213−1223.
(6) de Gennes, P. G. *The Physics of Liquid Crystals*, 2nd ed.; Clarendon Press: Oxford, England, 1993.
(7) Geissler, E. Dynamic Light Scattering on Gels. In *Dynamic Light Scattering*; Brown, W., Ed.; Clarendon Press: Oxford, England, 1993.
(8) Lindsey, C. P.; Patterson, G. D. *J. Chem. Phys* **1980**, *73*, 3348−3357.
(9) Bender, T. M.; Lewis, R. J.; Pecora, R. *Macromolecules* **1986**, *19*, 244−245.
(10) Lax, M.; Nelson, D. F. *J. Opt. Soc. Am.* **1975**, *65*, 668-675.
(11) Filippov, A. P.; Andreeva, L. N.; Barmatov, E. B.; Shibaev, V. P. *Mol. Cryst. Liq. Cryst.* **1997**, *299*, 143−148.
(12) Seiberle, H.; Stille, W.; Strobl, G. *Macromolecules* **1990**, *23*, 2008−2016.
(13) Götz, S.; Stille, W.; Strobl, G. *Macromolecules* **1993**, *26*, 1520−1528.
(14) Christoph, G.; Stille, W.; Strobl, G. *J. Chem. Phys.* **1993**, *99*, 3075−3081.
(15) Brochard, F. *J. Polym. Sci., Polym. Phys. Ed.* **1979**, *17*, 1367−1374.
(16) Raviol, A.; Stille, W.; Strobl, G. *J. Chem Phys.* **1995**, *103*, 3788−3794.
(17) Marrucci, G. *Mol. Cryst. Liq. Cryst. Lett.* **1982**, *72*, 153−161.
(18) Doi, M. J. *Polym. Sci., Part B: Polym. Phys.* **1981**, *19*, 229−243.
(19) Kirste, R. G.; Ohm, H. G. *Makromol. Rapid Commun.* **1985**, *6*, 179−185.
(20) Moussa, J. P.; Cotton, J. P.; Hardouin, P.; Keller, M.; Lambert, M.; Pepy, G.; Mauzac, M.; Richard, H. *J. Phys.* **1987**, *48*, 1079−1083.
(21) Noirez, J. P.; Cotton, J. P.; Hardouin, F.; Keller, P.; Moussa, F.; Pepy, G.; Strazielle, C. *Macromolecules* **1988**, *21*, 2889−2891.
(22) Pepy, G.; Noirez, L.; Keller, P.; Lambert, M.; Moussa, F.; Cotton, J.-P.; Strazielle, C.; Lapp, A.; Hardouin, F.; Mauzac, M.; Richard, H. *Makromol. Chem.* **1990**, *191*, 1383−1392.
(23) Mattoussi, H.; Ober, R.; Veyssie, M.; Finkelmann, H. *Europhys. Lett.* **1986**, *2* (3), 233−240.
(24) Yao, N.; Jamieson, A. M. *Macromolecules* **1997**, *30*, 5822−5831.
(25) Stinson, T. W.; Litster, J. D.; Clark, N. A. *J. Phys.* **1972**, *C1*, 69−75.

MA9911997